

Structure of a Perturbed Magnetic Reconnection Electron Diffusion Region in the Earth's Magnetotail

G. Cozzani^{1,*}, Yu. V. Khotyaintsev¹, D. B. Graham¹, J. Egedal², M. André¹, A. Vaivads³, A. Alexandrova⁴, O. Le Contel⁴, R. Nakamura⁵, S. A. Fuselier^{6,7}, C. T. Russell⁸, and J. L. Burch⁶

¹Swedish Institute of Space Physics, Uppsala 75121, Sweden

²Department of Physics, University of Wisconsin-Madison, Madison, Wisconsin 53706, USA

³Space and Plasma Physics, School of Electrical Engineering and Computer Science, KTH Royal Institute of Technology, Stockholm 11428, Sweden


⁴Laboratoire de Physique des Plasmas, CNRS, Sorbonne Université, Université Paris-Saclay, Observatoire de Paris, École Polytechnique Institut Polytechnique de Paris, Palaiseau 91128, France

⁵Space Research Institute, Austrian Academy of Sciences, Graz 8042, Austria

⁶Southwest Research Institute, San Antonio, Texas 78238, USA

⁷University of Texas at San Antonio, San Antonio, Texas 78249, USA

⁸University of California, Los Angeles, California 90095, USA

 (Received 28 March 2021; revised 22 September 2021; accepted 7 October 2021; published 15 November 2021)

We report *in situ* observations of an electron diffusion region (EDR) and adjacent separatrix region in the Earth's magnetotail. We observe significant magnetic field oscillations near the lower hybrid frequency which propagate perpendicularly to the reconnection plane. We also find that the strong electron-scale gradients close to the EDR exhibit significant oscillations at a similar frequency. Such oscillations are not expected for a crossing of a steady 2D EDR, and can be explained by a complex motion of the reconnection plane induced by current sheet kinking propagating in the out-of-reconnection-plane direction. Thus, all three spatial dimensions have to be taken into account to explain the observed perturbed EDR crossing. These results shed light on the interplay between magnetic reconnection and current sheet drift instabilities in electron-scale current sheets and highlight the need for adopting a 3D description of the EDR, going beyond the two-dimensional and steady-state conception of reconnection.

DOI: [10.1103/PhysRevLett.127.215101](https://doi.org/10.1103/PhysRevLett.127.215101)

Magnetic reconnection is a fundamental plasma process that results in the topological reconfiguration of the magnetic field and the concurrent energization and acceleration of plasma species [1]. Reconnection is found in a variety of environments in space and astrophysical plasmas [2] and dedicated laboratory experiments [3,4]. A crucial constituent of the collisionless reconnection process is the electron diffusion region (EDR), where the demagnetization of both ions and electrons enables the magnetic field topology change. As a result, the processes that take place in the EDR affect the system up to its global magnetohydrodynamics scales. Despite their central role, these processes are still largely unknown. The contribution of plasma waves and instabilities to the EDR dynamics as well as to the overall reconnection process remains unclear [5,6]. Waves and instabilities operating in the center of the current sheet could affect the two-dimensional, steady, and laminar reconnection picture. For guide-field reconnection, in particular, the role of streaming instabilities leading to turbulence development at the reconnection site has been discussed in simulation studies [7,8] and electrostatic turbulence promoting electron heating is observed at a magnetopause EDR [9].

A class of current sheet drift instabilities with frequencies in the lower hybrid frequency range has been extensively studied in the last decades. The electrostatic lower hybrid drift instability (LHDI) is one of the modes that has initially received most of the attention since it could potentially provide anomalous resistivity sustaining the reconnection electric field [10,11]. However, spacecraft observations at the magnetopause [12–14] and magnetotail [15,16] suggest that electrostatic LHDI modes could not supply the necessary resistivity, consistent with the fact that these modes develop at the edges of the current sheet but are stabilized in the center [17]. On the other hand, eigenmode analysis and kinetic simulations [18–20] show that electromagnetic modes in the lower hybrid frequency range can penetrate into the center of the current layer and induce current sheet kinking. Such modes are characterized by lower growth rates and longer wavelength compared to the electrostatic modes. Among these modes, the electromagnetic LHDI and the modified two stream instability (MTSI) [21,22] have been considered, for a long time, two separate instabilities. However, local [23] and nonlocal theories [20] provide a unified formulation of LHDI and MTSI. A local theoretical model [24,25], reproducing both

LHDI and MTSI, was developed to interpret the electromagnetic fluctuations observed within a reconnecting current sheet in the magnetic reconnection experiment (MRX) [26]. The fluctuations observed at MRX are identified as obliquely propagating electromagnetic LHDI modes [24].

Before the launch of the Magnetospheric Multiscale (MMS) mission [27], observational evidence of these instabilities occurring at the EDR were prevented by the lower resolution of the available particle measurements and by the limited knowledge of the EDR and related electron-scale processes. Electrostatic [28] and electromagnetic [29] lower hybrid drift waves (LHDWs) in the EDR have been investigated only recently. However, how these instabilities affect the structure of the EDR is still unknown.

In this Letter, we report MMS observations of a magnetotail electron diffusion region and adjacent separatrix region characterized by unexpected electric field, electron velocity and magnetic field oscillations. We compare 2D fully kinetic simulations and four-spacecraft observations to investigate the mechanism responsible for the observed oscillations.

MMS encountered an EDR on August 10, 2017 at 12:18:33 UTC when it was located in the Earth's magnetotail at $[-15.2, 4.6, 3.1]_{\text{GSM}} R_E$ (in the Geocentric Solar Magnetospheric system). The indicative signatures of an EDR [30–32]—including super-Alfvénic electron jets, enhanced electron agyrotropy, electron demagnetization, intense energy conversion, and crescent-shaped electron distribution functions—are observed [33]. During this event, MMS stays mostly in the plasma sheet ($B \sim 7$ nT and $n \sim 0.17$ cm $^{-3}$). A weak guide field $B_g \sim 2$ nT $\sim 0.13 B_{\text{inflow}}$ is present (B_{inflow} is the inflow magnetic field computed in the interval 12:21:20–12:21:40 [33]). The mean interspacecraft separation, ~ 20 km, is comparable to the electron inertial length, $d_e \sim 13$ km. As a first step, we determine the appropriate LMN coordinate system and establish the MMS trajectory relative to the EDR by adopting methods reported in Refs. [34,35]. For this we use a 2D-3V kinetic particle-in-cell (PIC) simulation performed with the VPIC code [36] which mimics the MMS event (simulation run featuring upstream $\beta_{e,\infty} = 0.09$ and $B_g = 0.1$ [37]). The realistic ion-to-electron mass ratio $m_i/m_e = 1836$ allows us to establish a one-to-one correspondence between the dimensionless units of the simulation and the physical units of MMS data.

Figure 1 shows an overview of the EDR crossing. All the quantities are shown in the LMN coordinate system ($L = [0.96, -0.15, -0.22]$, $M = [0.17, 0.98, 0.03]$, $N = [0.22, -0.07, 0.97]$ in GSM, obtained via an optimization approach aided by simulation data [34]). The MMS trajectory relative to the EDR is shown in Fig. 1(i). The trajectory is reconstructed in interval $A - F$ (12:18:28.9–12:18:36.5) of Fig. 1. The part of trajectory corresponding to interval 12:18:28.9–12:18:33.8 (from the A -labeled line to the magenta line in Fig. 1) is reconstructed by adapting

the method of Ref. [35] to include the electron velocity $v_{e,M}$ and the electron temperature anisotropy. For the part of the trajectory corresponding to interval 12:18:33.8–12:18:36.5 (from the magenta line to the F -labeled line in Fig. 1), we use the method of Ref. [34] (including E_N and B_L) which allows us to reproduce the observed electric field oscillations.

MMS is initially located southward and tailward of the reconnection site, corresponding to $B_L < 0$ [Fig. 1(a)], $B_N < 0$ [Fig. 1(c)] and $V_{i,L} < 0$ (not shown). Then, MMS crosses the diffusion region diagonally so that B_L and B_N change from negative to positive. MMS samples mainly the positive lobes of the Hall quadrupolar field [$B_M > B_g$, Fig. 1(b)]. Figure 1(g) shows the electron temperature anisotropy $T_{e,\parallel}/T_{e,\perp}$, where parallel and perpendicular refer to the local magnetic field direction. The $T_{e,\parallel}/T_{e,\perp}$ peak observed at 12:18:30.5 indicates that MMS performed a brief excursion into the inflow region, where $T_{e,\parallel}/T_{e,\perp}$ is expected to increase [42,43], before approaching the inner EDR (interval $C - D$) [44]. Interestingly, during the current sheet crossing (interval $B - E$), MMS observes significant magnetic field oscillations δB [Fig. 1(h)] reaching $\sim 20\%$ of the upstream magnetic field in the plasma sheet (~ 7 nT). Applying the timing method [45] on the sharp B_L variation in interval 12:18:32.0–12:18:33.3 we estimate the current layer width to be $d_{cs} \sim 2d_e$, in agreement with Ref. [33]. This small width implies that MMS crossed an electron scale current sheet.

While the typical signatures of an EDR encounter are observed overall, the multispacecraft analysis of electric and velocity fields along the spacecraft trajectory allows us to identify signatures which are distinctive of this event. Figure 1(f) shows the normal component of the electric field, E_N , exhibiting a bipolar behavior consistent with Hall dynamics. While the different spacecraft see similar E_N in interval $A - D$ (12:18:28.9–12:18:33.4), significant differences between the spacecraft are observed in interval $D - F$ (12:18:33.4–12:18:36.5). The largest difference is observed between spacecraft with the largest separation in the N direction [MMS1 and MMS2, Fig. 1(j)] while spacecraft which are close to each other in the N direction and separated both in L (MMS2 and MMS4) and M direction (MMS2 and MMS4, not shown) observe nearly identical signals. The difference between E_N measured at MMS1 and MMS2 (which are only $1.1d_e$ apart along the N direction) reaches a maximum value of ~ 30 mV/m. Analogously to the differences in E_N , also significant differences are observed in $v_{e,L}$ [Fig. 1(e)], reaching 2000 km/s. These differences indicate the presence of strong gradients on spatial scales $\sim d_e$.

However, the most intriguing feature of this EDR crossing is the presence of large fluctuations in E_N , $v_{e,L}$ along the separatrix (region $D - F$) and of δB in the current sheet center (interval $B - E$). Such oscillations are not expected for a smooth crossing of a laminar EDR, and their

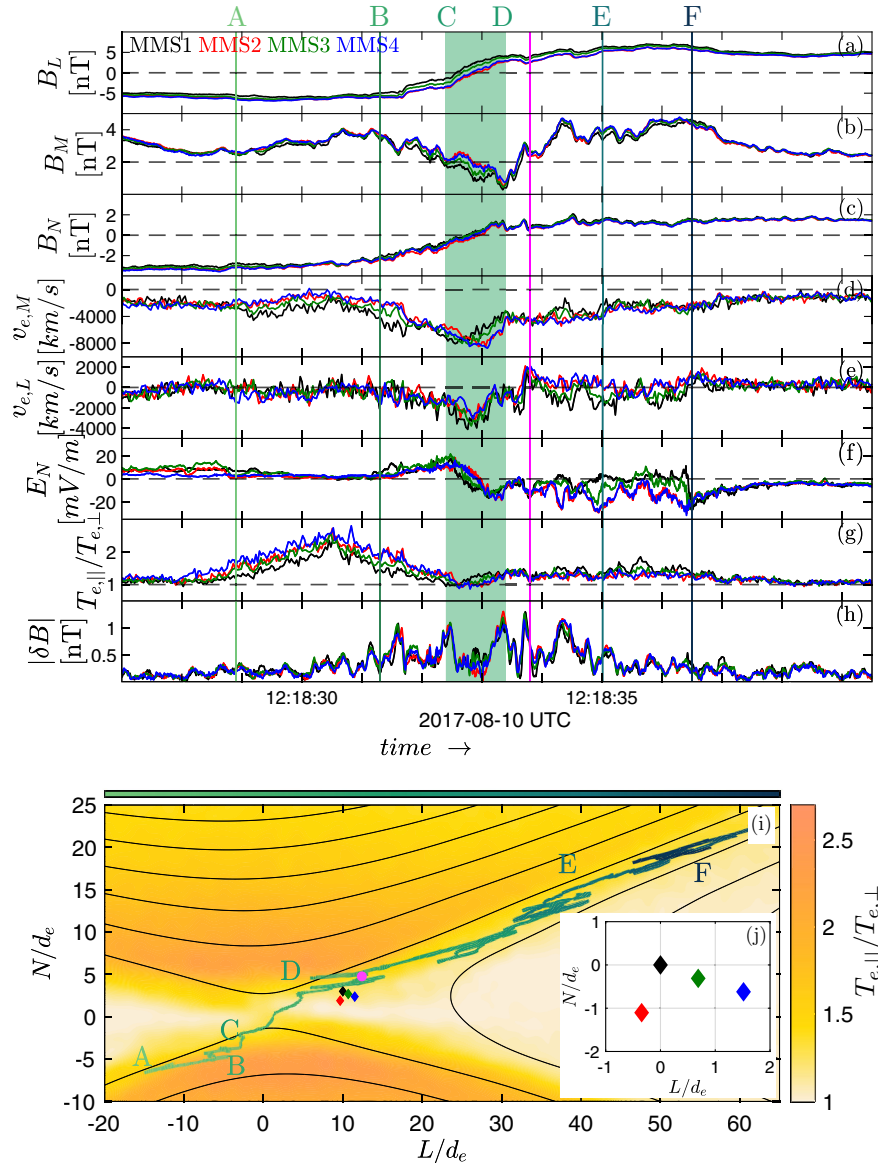


FIG. 1. Top: Four spacecraft (a) B_L , (b) B_M , and (c) B_N measured by FGM [38]; (d) $v_{e,M}$ and (e) $v_{e,L}$ from FPI [39]; (f) E_N from EDP [40,41]; (g) $T_{e,||}/T_{e,\perp}$; (h) $|\delta B|$ computed high-pass filtering FGM data with $f > 0.5$ Hz (the high-pass filter allows us to separate the scale associated with the fluctuations from the scale associated with the magnetic field variations due to the current sheet crossing). The green shaded interval indicates the inner EDR. Bottom: (i) 2D PIC simulation data of $T_{e,||}/T_{e,\perp}$ with the reconstructed MMS trajectory crossing the EDR. The magnetic flux contour lines are superposed; (j) spacecraft position relative to MMS1 in the LN plane.

presence indicates that the EDR crossing is perturbed by some process. We investigate these oscillations in detail in order to identify this process.

Figure 2 focuses on the separatrix region characterized by the strong gradients. Both $v_{e,L}$ and E_N [Figs. 2(b) and 2(c)] show very different profiles at each spacecraft. Notably, MMS2 and MMS4 observe a strongly fluctuating and mostly negative E_N while E_N is mostly positive for MMS1 and the fluctuations are not as prominent. Indeed, the difference between E_N measured by MMS1 and MMS2 [$\Delta E_N = E_{N,MMS2} - E_{N,MMS1}$, Fig. 2(d)] and analogously $\Delta v_{e,L} = v_{e,L,MMS2} - v_{e,L,MMS1}$ show large variations. Such

large variations in the observed gradients can be either caused by kinking of the current sheet as a whole or by temporal variations of the gradients at electron scales, or by a combination of the two.

Figures 2(e) and 2(f) show 2D PIC simulation data of E_N and $v_{e,L}$ in the LN plane. The location of MMS corresponding to the E -labeled line is shown in Figs. 2(a)–2(d). The simulation data [Fig. 2(e) and 2(f)] exhibit large differences in E_N and $v_{e,L}$ at the different spacecraft locations, thus electron scale gradients, as the ones observed *in situ*, are also present in the simulation. However, considering the laminar character of the

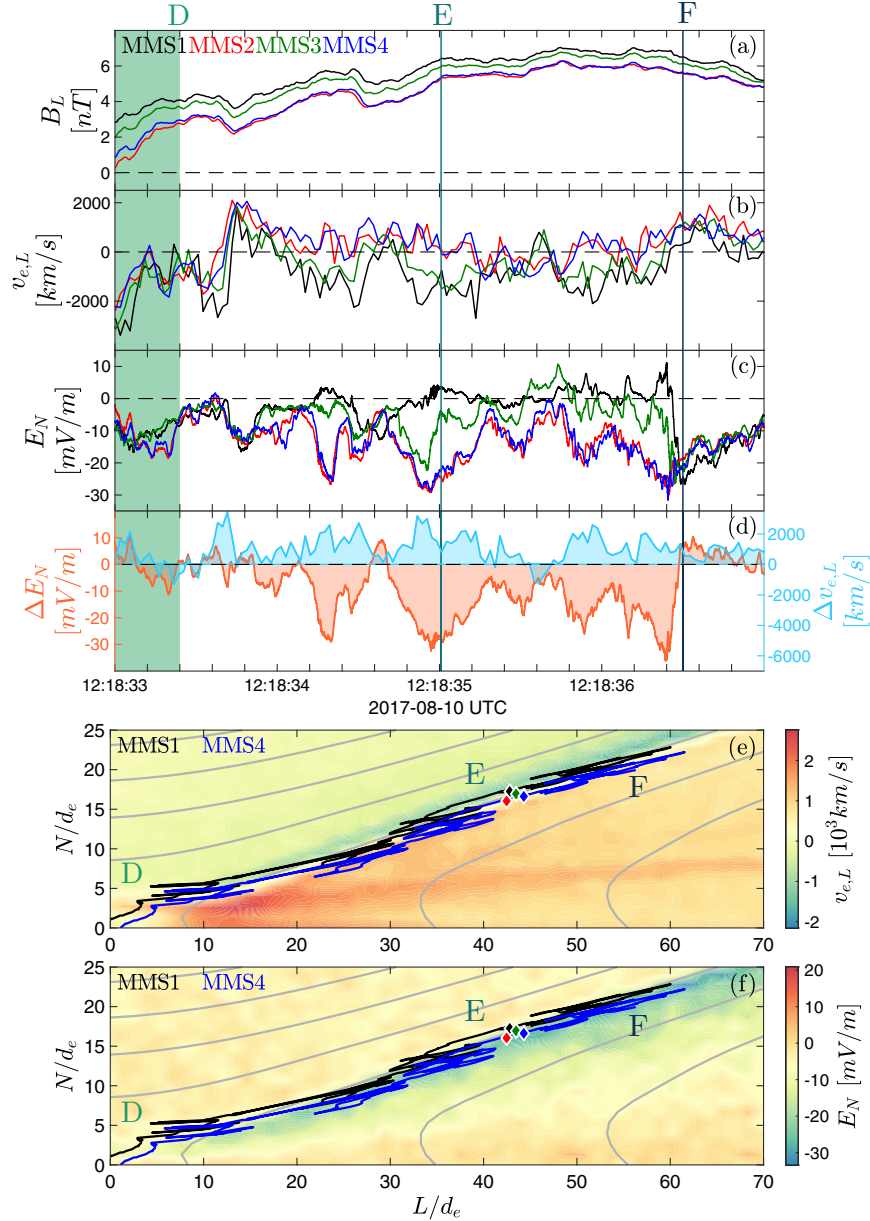


FIG. 2. Four spacecraft MMS observations: (a) B_L ; (b) $v_{e,L}$; (c) E_N ; (d) $\Delta E_N = E_{N,MMS2} - E_{N,MMS1}$ and $\Delta v_{e,L} = v_{e,L,MMS2} - v_{e,L,MMS1}$. PIC simulation: contour plot of (e) $v_{e,L}$ and (f) E_N . The black (blue) line represents MMS1 (MMS4) trajectory.

simulation data, if one were to consider a smooth MMS trajectory across a steady-state 2D reconnection plane (see, e.g., [32,34]), one would expect the difference between E_N and $v_{e,L}$ observed at different spacecraft to be rather constant and the related gradients to be uniform along the separatrix. This is in striking contrast with the large variations in the gradients observed by MMS. The 2D simulation can be matched to the *in situ* data only if we use a rather complex trajectory [Figs. 2(e) and 2(f)]. This trajectory is overall tangential to the separatrix, yet it exhibits several back-and-forth motions which are necessary to reproduce the oscillating ΔE_N and $\Delta v_{e,L}$ observed *in situ*.

In order to identify the process responsible for the complex EDR crossing, we analyze the observed $\delta\mathbf{B}$ fluctuations [see Fig. 1(h)]. Figure 3(a) shows that the $\delta\mathbf{B}$ fluctuations, with similar amplitude in all three components, are present in the current sheet center, where the current density peaks [Fig. 3(b), yellow shaded interval 12:18:30.3–12:18:36.5]. In addition, the observed $\delta\mathbf{B}$ fluctuations are compressional (not shown). Figures 3(c) and 3(d) show the wavelet power spectra of the electric and magnetic fields observed by MMS1. Both the magnetic and electric powers clearly drop for frequencies $f > f_{LH}$ ($f_{LH} \approx \sqrt{f_{ci}f_{c,e}}$ is the lower hybrid frequency) and in the inner EDR the waves have $f \sim f_{LH}$. The parameter

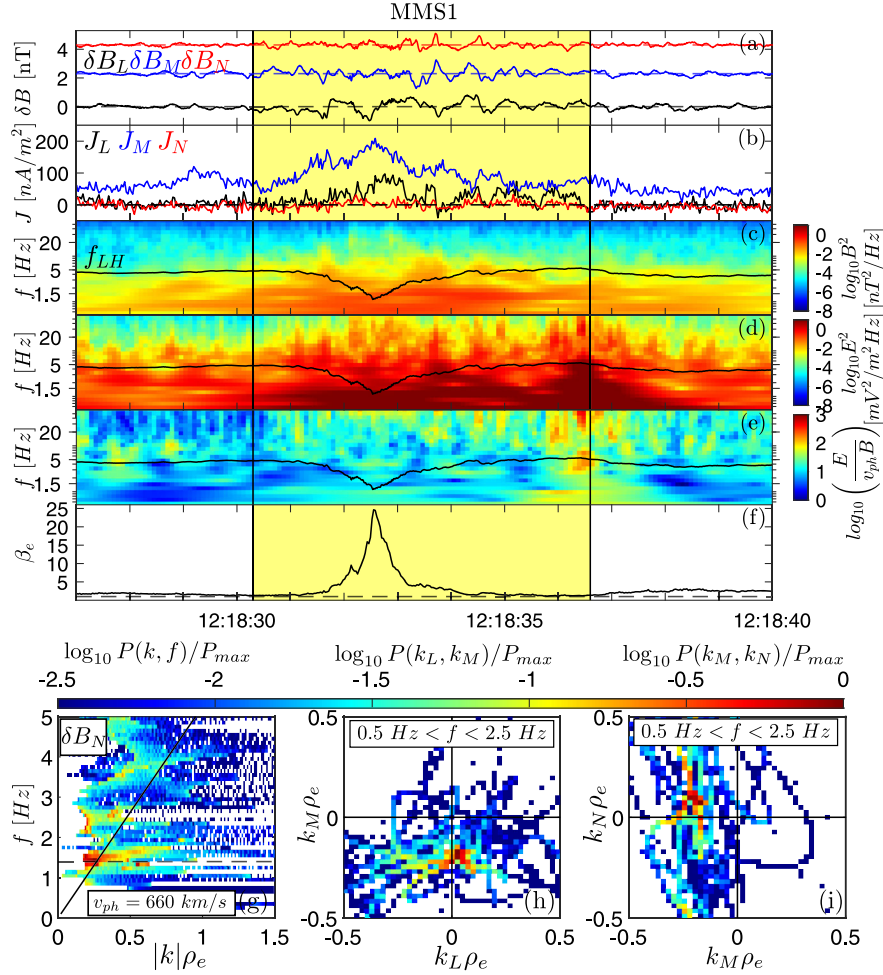


FIG. 3. Top: (a) three components of $\delta\mathbf{B}$. Offsets of 2.3 nT and 4.3 nT are added to δB_M and δB_N , respectively; (b) \mathbf{J} calculated from particle moments. Spectrum of (c) \mathbf{B} wave power; (d) \mathbf{E} wave power; (e) $\log_{10}[(E/B)(1/v_{ph})]$. (f) β_e . The black line indicates f_{LH} . Bottom: normalized power of magnetic field fluctuations δB_N versus (g) $|k|\rho_e$ and frequency; (h) $k_L\rho_e$ and $k_M\rho_e$ ($0.5 \text{ Hz} < f < 2.5 \text{ Hz}$); (i) $k_M\rho_e$ and $k_N\rho_e$ ($0.5 \text{ Hz} < f < 2.5 \text{ Hz}$). The dashed line in (g) corresponds to $f = 1.4 \text{ Hz}$.

$(E/B)(1/v_{ph})$ [Fig. 3(e)], where v_{ph} is the phase speed of the observed waves [see Fig. 3(g)], is used to quantify the electrostatic and electromagnetic component of the waves. Theoretically, the parameter $(E/B)(1/v_{ph}) \rightarrow \infty$ for purely electrostatic waves. Averaging this parameter in the yellow shaded interval of Fig. 3 and in the frequency range $1 \text{ Hz} < f < 5 \text{ Hz}$, we obtain a mean value of $(E/B)(1/v_{ph}) \sim 15$ which is much smaller than the typical value observed in the quasioleostatic case. For example, $(E/B)(1/v_{ph}) \sim 400$ ($0.3 < f/f_{LH} < 0.8$) for the quasioleostatic fluctuations reported in Ref. [46]. Thus, the fluctuations in the center of the reconnecting current sheet are characterized by a significant electromagnetic component.

To better characterize these fluctuations, we compute the dispersion relation from the phase differences of δB_N between spacecraft pairs, using multispacecraft interferometry [46,47]. Figure 3(g) shows that the normalized power $P(f, k)/P_{max}$ peaks at $f \sim 1.4 \text{ Hz}$ (black dashed

line) which is close to f_{LH} at the current sheet center. The wave number at the $P(f, k)/P_{max}$ peak is $k\rho_e \sim 0.3$ (and $k\sqrt{\rho_e\rho_i} \sim 2.7$, where $\rho_e \sim 24 \text{ km}$ and $\rho_i \sim 2150 \text{ km}$ are the electron and ion gyroradius averaged over the yellow shaded region of Fig. 3) which corresponds to phase speed $v_{ph} \sim 660 \text{ km/s}$ and wavelength $\lambda \sim 500 \text{ km}$. Figures 3(h) and 3(i) shows that the wave vector \mathbf{k} is directed mainly along the M direction, i.e., antialigned with the direction of the current and perpendicular to the reconnection plane. The average direction of propagation of the fluctuations is $\hat{\mathbf{k}} = [0.12, -0.92, 0.38]$ in LMN coordinates and it is mainly perpendicular to the magnetic field direction ($\theta_k = \arccos[(\mathbf{k} \cdot \mathbf{B})/(\|\mathbf{k}\|\|\mathbf{B}\|)] \sim 70^\circ$, not shown). Similar results are obtained if a different component of $\delta\mathbf{B}$ is considered for the analysis. These signatures are consistent with lower hybrid drift fluctuations propagating in the out-of-reconnection-plane direction.

The $\delta\mathbf{B}$ fluctuations in the current sheet center and the electric and velocity field fluctuations at the separatrix have

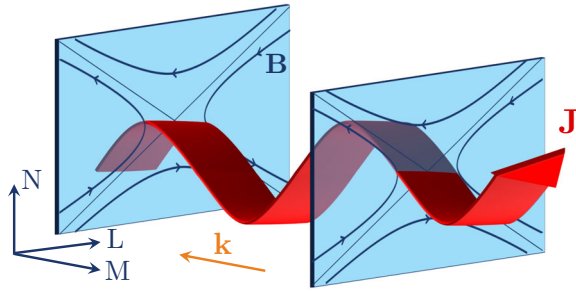


FIG. 4. Schematic representation of the kinking of the electron scale current sheet propagating in the out-of-reconnection-plane direction (not to scale).

similar time scales which are comparable to the lower hybrid frequency [Figs. 3(c) and 3(d) and Fig. 2(d)]. This similarity suggests that they are related to each other. As shown in Fig. 2, we can match the observed oscillating ΔE_N and $\Delta v_{e,L}$ to the steady-state 2D reconnection structure if we employ a complex motion of the 2D reconnection plane. Both such complex motion and the $\delta \mathbf{B}$ fluctuations in the current sheet center can be produced by kinking of the current sheet propagating in the out-of-reconnection-plane direction (see a qualitative representation in Fig. 4). On the other hand, given the electron-scale interspacecraft separation which does not allow the sampling of the larger scales, we cannot establish whether the oscillations shown in Figs. 2(b)–2(d) are indeed produced exclusively by the rigid motion of the reconnection plane, or if a more complex behavior including time evolution is present. However, the analyses discussed above provide evidence that the current sheet kinking is perturbing the EDR crossing. Hence, we conclude that the time-dependent processes, if present, are secondary sources of the observed EDR crossing perturbation.

The fluctuations observed during the EDR crossing are related to one of the various drift instabilities that are eigenoscillations resulting in current sheet kinking [18,19]. Several modes that have been considered as distinguished in the past actually belong to the same class of instabilities ranging from the electrostatic LHDI (fast growing, short-wavelength mode with $k\rho_e \sim 1$) localized at the edges of the current sheet [17] to the electromagnetic, longer-wavelength modes with $k\sqrt{\rho_i\rho_e} \sim 1$ located close to the current sheet center which arise in later phases of the instability [18,19,48–50]. In the event reported here, MMS observe obliquely propagating electromagnetic fluctuations with rather long wavelength ($k\rho_e \sim 0.3$ is smaller than the typical $k\rho_e \sim 0.5$ –1 observed for LHDW at the magnetopause [14,51]) located within the EDR. The observed fluctuations are somewhat consistent with the obliquely propagating electromagnetic drift instability [24] which can occur at higher β_e observed in the current sheet center [see Fig. 3(e)]. The local theory of Ref. [24] was developed in order to explain the electromagnetic fluctuations that have been observed at the MRX [26].

Despite the similarities, the comparison between our observations and the analytical and simulation studies [18,19,24] or laboratory [26] and spacecraft observations [52] focusing on current sheet instabilities is constrained by the fact that the current sheet thickness in these studies is $d_{cs} \sim d_i$ while our event presents a very thin current sheet $d_{cs} \sim 2d_e = 0.05d_i$. Also, the plasma considered in previous studies is usually homogeneous [53], reconnection is not present [18,19,24] or it is asymmetric [54]. Further detailed comparison with theoretical models [18,19,24] are beyond the scope of this Letter and will be investigated in future work. Independently of the specific instability operating in the current sheet, when the direction of propagation is perpendicular to the reconnection plane the out-of-plane direction cannot be treated as an invariant axis of the system. Thus, a 3D description is required to understand the dynamics of the process.

In conclusion, we report MMS observations of a perturbed EDR crossing. We observe oscillations of the electron-scale gradients at the separatrix and magnetic field fluctuations in the current sheet center. These features are not expected for a simple crossing of a steady-state 2D EDR. We find an overall good agreement between the observations and 2D PIC simulations of reconnection, but we can only match the observed oscillations to the 2D model if we consider a complex motion of the spacecraft in the fixed 2D reconnection plane. We attribute such complex motion to a kinking of the current sheet associated with electromagnetic drift instability propagating in the out-of-reconnection-plane direction. Despite the overall quasi-2D geometry of the event, these results suggest that we need to take into account the three-dimensionality of the system to fully understand the observed EDR crossing. Further *in situ* data analysis and three-dimensional simulations enabling the out-of-plane dynamics are needed to establish the role of current sheet instabilities in affecting the EDR structure.

MMS data are available at the MMS Science Data Center, see Ref. [55].

We thank the entire MMS team and instruments principal investigators for data access and support. We gratefully thank W. Daughton for running the simulations. This work was supported by the Swedish Research Council, Grants No. 2016-05507 and No. 2018-03569, and the Swedish National Space Agency, Grants No. 128/17 and No. 144/18.

*giuliac@irfu.se

- [1] V. M. Vasyliunas, Theoretical models of magnetic field line merging, *Rev. Geophys.* **13**, 303 (1975).
- [2] E. G. Zweibel and M. Yamada, Magnetic reconnection in astrophysical and laboratory plasmas, *Annu. Rev. Astron. Astrophys.* **47**, 291 (2009).
- [3] M. Yamada, H. Ji, S. Hsu, T. Carter, R. Kulsrud, N. Bretz, F. Jobs, Y. Ono, and F. Perkins, Study of driven magnetic

- reconnection in a laboratory plasma, *Phys. Plasmas* **4**, 1936 (1997).
- [4] C. Forest *et al.*, The Wisconsin plasma astrophysics laboratory, *J. Plasma Phys.* **81**, 345810501 (2015).
- [5] M. Fujimoto, I. Shinohara, and H. Kojima, Reconnection and waves: A review with a perspective, *Space Sci. Rev.* **160**, 123 (2011).
- [6] Y. V. Khotyaintsev, D. B. Graham, C. Norgren, and A. Vaivads, Collisionless magnetic reconnection and waves: Progress review, *Rev. Front. Astron. Space Sci.* **6**, 70 (2019).
- [7] J. F. Drake, M. Swisdak, C. Cattell, M. A. Shay, B. N. Rogers, and A. Zeiler, Formation of electron holes and particle energization during magnetic reconnection, *Science* **299**, 873 (2003).
- [8] H. Che, How anomalous resistivity accelerates magnetic reconnection, *Phys. Plasmas* **24**, 082115 (2017).
- [9] Yu. V. Khotyaintsev, D. B. Graham, K. Steinvall, L. Alm, A. Vaivads, A. Johlander, C. Norgren, W. Li, A. Divin, H. S. Fu, K.-J. Hwang, J. L. Burch, N. Ahmadi, O. Le Contel, D. J. Gershman, C. T. Russell, and R. B. Torbert, Electron Heating by Debye-Scale Turbulence in Guide-Field Reconnection, *Phys. Rev. Lett.* **124**, 045101 (2020).
- [10] J. D. Huba, N. T. Gladd, and K. Papadopoulos, The lower-hybrid-drift instability as a source of anomalous resistivity for magnetic field line reconnection, *Geophys. Res. Lett.* **4**, 125 (1977).
- [11] C. Cattell, J. Wygant, F. S. Mozer, T. Okada, K. Tsuruda, S. Kokubun, and T. Yamamoto, ISEE 1 and Geotail observations of low-frequency waves at the magnetopause, *J. Geophys. Res.* **100**, 11823 (1995).
- [12] S. D. Bale, F. S. Mozer, and T. Phan, Observation of lower hybrid drift instability in the diffusion region at a reconnecting magnetopause, *Geophys. Res. Lett.* **29**, 33-1 (2002).
- [13] A. Vaivads, M. André, S. C. Buchert, J.-E. Wahlund, A. N. Fazakerley, and N. Cornilleau-Wehrin, Cluster observations of lower hybrid turbulence within thin layers at the magnetopause, *Geophys. Res. Lett.* **31**, L03804 (2004).
- [14] D. B. Graham *et al.*, Lower hybrid waves in the ion diffusion and magnetospheric inflow regions, *J. Geophys. Res.* **122**, 517 (2017).
- [15] J. P. Eastwood, T. D. Phan, S. D. Bale, and A. Tjulin, Observations of Turbulence Generated by Magnetic Reconnection, *Phys. Rev. Lett.* **102**, 035001 (2009).
- [16] M. Zhou *et al.*, Observation of waves near lower hybrid frequency in the reconnection region with thin current sheet, *J. Geophys. Res.* **114**, A02216 (2009).
- [17] R. C. Davidson, N. T. Gladd, C. S. Wu, and J. D. Huba, Effects of finite plasma beta on the lower-hybrid-drift instability, *Phys. Fluids* **20**, 301 (1977).
- [18] W. Daughton, Electromagnetic properties of the lower-hybrid drift instability in a thin current sheet, *Phys. Plasmas* **10**, 3103 (2003).
- [19] P. H. Yoon, A. T. Y. Lui, and M. I. Sitnov, Generalized lower-hybrid drift instabilities in current-sheet equilibrium, *Phys. Plasmas* **9**, 1526 (2002).
- [20] P. H. Yoon and A. T. Y. Lui, Lower-hybrid-drift and modified-two-stream instabilities in current sheet equilibrium, *J. Geophys. Res.* **109**, A02210 (2004).
- [21] J. B. Hsia, S. M. Chiu, M. F. Hsia, R. L. Chou, and C. S. Wu, Generalized lower-hybrid-drift instability, *Phys. Fluids* **22**, 1737 (1979).
- [22] J. B. McBride, E. Ott, J. P. Boris, and J. H. Orens, Theory and simulation of turbulent heating by the modified two-stream instability, *Phys. Fluids* **15**, 2367 (1972).
- [23] O. J. G. Silveira, L. F. Ziebell, R. Gaelzer, and P. H. Yoon, Unified formulation for inhomogeneity-driven instabilities in the lower-hybrid range, *Phys. Rev. E* **65**, 036407 (2002).
- [24] H. Ji, R. Kulsrud, W. Fox, and M. Yamada, An obliquely propagating electromagnetic drift instability in the lower hybrid frequency range, *J. Geophys. Res.* **110**, A08212 (2005).
- [25] R. Kulsrud, H. Ji, W. Fox, and M. Yamada, An electromagnetic drift instability in the magnetic reconnection experiment and its importance for magnetic reconnection, *Phys. Plasmas* **12**, 082301 (2005).
- [26] H. Ji, S. Terry, M. Yamada, R. Kulsrud, A. Kuritsyn, and Y. Ren, Electromagnetic Fluctuations during Fast Reconnection in a Laboratory Plasma, *Phys. Rev. Lett.* **92**, 115001 (2004).
- [27] J. L. Burch, T. E. Moore, R. B. Torbert, and B. L. Giles, Magnetospheric multiscale overview and science objectives, *Space Sci. Rev.* **199**, 5 (2016).
- [28] L.-J. Chen, S. Wang, O. Le Contel, A. Rager, M. Hesse, J. Drake *et al.*, Lower-Hybrid Drift Waves Driving Electron Nongyrotropic Heating and Vortical Flows in a Magnetic Reconnection Layer, *Phys. Rev. Lett.* **125**, 025103 (2020).
- [29] J. Yoo *et al.*, Lower hybrid drift waves during guide field reconnection, *Geophys. Res. Lett.* **47**, e2020GL087192 (2020).
- [30] J. L. Burch *et al.*, Electron-scale measurements of magnetic reconnection in space, *Science* **352**, aaf2939 (2016).
- [31] J. M. Webster *et al.*, Magnetospheric multiscale dayside reconnection electron diffusion region events, *J. Geophys. Res.* **123**, 4858 (2018).
- [32] R. B. Torbert *et al.*, Electron-scale dynamics of the diffusion region during symmetric magnetic reconnection in space, *Science* **362**, 1391 (2018).
- [33] M. Zhou *et al.*, Observations of an electron diffusion region in symmetric reconnection with weak guide field, *Astrophys. J.* **870**, 34 (2019).
- [34] J. Egedal, J. Ng, A. Le, W. Daughton, B. Wetherington, J. Dorelli, D. Gershman, and A. Rager, Pressure Tensor Elements Breaking the Frozen-In Law During Reconnection in Earth's Magnetotail, *Phys. Rev. Lett.* **123**, 225101 (2019).
- [35] J. R. Shuster *et al.*, Hodographic approach for determining spacecraft trajectories through magnetic reconnection diffusion regions, *Geophys. Res. Lett.* **44**, 1625 (2017).
- [36] K. J. Bowers, B. J. Albright, L. Yin, B. Bergen, and T. J. T. Kwan, Ultrahigh performance three-dimensional electromagnetic relativistic kinetic plasma simulation, *Phys. Plasmas* **15**, 055703 (2008).
- [37] A. Le, J. Egedal, O. Ohia, W. Daughton, H. Karimabadi, and V. S. Lukin, Regimes of the Electron Diffusion Region in Magnetic Reconnection, *Phys. Rev. Lett.* **110**, 135004 (2013).
- [38] C. T. Russell *et al.*, The magnetospheric multiscale magnetometers, *Space Sci. Rev.* **199**, 189 (2016).
- [39] C. Pollock *et al.*, Fast plasma investigation for magnetospheric multiscale, *Space Sci. Rev.* **199**, 331 (2016).
- [40] R. E. Ergun *et al.*, The axial double probe and fields signal processing for the MMS mission, *Space Sci. Rev.* **199**, 167 (2016).

- [41] P.-A. Lindqvist *et al.*, The spin-plane double probe electric field instrument for MMS, *Space Sci. Rev.* **199**, 137 (2016).
- [42] J. Egedal, W. Fox, N. Katz, M. Porkolab, M. Øieroset, R. P. Lin, W. Daughton, and J. F. Drake, Evidence and theory for trapped electrons in guide field magnetotail reconnection, *J. Geophys. Res.* **113**, A12207 (2008).
- [43] J. Egedal, A. Le, and W. Daughton, A review of pressure anisotropy caused by electron trapping in collisionless plasma, and its implications for magnetic reconnection, *Phys. Plasmas* **20**, 061201 (2013).
- [44] H. Karimabadi, W. Daughton, and J. Scudder, Multi-scale structure of the electron diffusion region, *Geophys. Res. Lett.* **34**, L13104 (2007).
- [45] C. C. Harvey, in *Analysis Methods for Multi-Spacecraft Data*, edited by G. Paschmann and P. Daly, ISSI Scientific Reports Series Vol. 1 (ESA/ISSI, Bern, 1998), p. 307.
- [46] D. B. Graham *et al.*, Universality of lower hybrid waves at Earth's magnetopause, *J. Geophys. Res.* **124**, 8727 (2019).
- [47] D. B. Graham, Y. V. Khotyaintsev, A. Vaivads, and M. André, Electrostatic solitary waves and electrostatic waves at the magnetopause, *J. Geophys. Res.* **121**, 3069 (2016).
- [48] I. Shinohara, H. Suzuki, M. Fujimoto, and M. Hoshino, Rapid Large-Scale Magnetic-Field Dissipation in a Collisionless Current Sheet via Coupling between Kelvin-Helmholtz and Lower-Hybrid Drift Instabilities, *Phys. Rev. Lett.* **87**, 095001 (2001).
- [49] H. Suzuki, M. Fujimoto, and I. Shinohara, Current-sheet kink instability at ion-electron hybrid scale, *Adv. Space Res.* **30**, 2663 (2002).
- [50] M. Scholer, I. Sidorenko, C. H. Jaroschek, and R. A. Treumann, Onset of collisionless magnetic reconnection in thin current sheets: Three-dimensional particle simulations, *Phys. Plasmas* **10**, 3521 (2003).
- [51] Y. V. Khotyaintsev *et al.*, Electron jet of asymmetric reconnection, *Geophys. Res. Lett.* **43**, 5571 (2016).
- [52] Y. Asano, T. Mukai, M. Hoshino, Y. Saito, H. Hayakawa, and T. Nagai, Evolution of the thin current sheet in a substorm observed by Geotail, *J. Geophys. Res.* **108**, 1189 (2003).
- [53] C. S. Wu, Y. M. Zhou, Shih-Tung Tsai, and S. C. Guo, A kinetic cross-field streaming instability, *Phys. Fluids* **26**, 1259 (1983).
- [54] V. Roytershteyn, W. Daughton, H. Karimabadi, and F. S. Mozer, Influence of the Lower-Hybrid Drift Instability on Magnetic Reconnection in Asymmetric Configurations, *Phys. Rev. Lett.* **108**, 185001 (2012).
- [55] <https://lasp.colorado.edu/mms/sdc/public/>.